Optimization of a 60° waveguide bend in InP-based 2D planar photonic crystals

Patric Strasser,[1,*] Glen Stark,[1] Franck Robin,[1] Daniel Erni,[1,3] Katharina Rauscher,[2] Robert Wüest,[1] and Heinz Jäckel[1]

[1]*Electronics Laboratory, ETH Zurich, 8092 Zurich, Switzerland*
[2]*Laboratory for Electromagnetic Fields and Microwave Electronics, ETH Zurich, 8092 Zurich, Switzerland*
[3]*General and Theoretical Electrical Engineering (ATE), Faculty of Engineering, University of Duisburg-Essen, 47048 Duisburg, Germany*
**Corresponding author: strasser@ife.ee.ethz.ch*

Received September 4, 2007; accepted October 7, 2007;
posted November 16, 2007 (Doc. ID 87197); published December 21, 2007

We present a novel design for a *W*1 (one missing row of holes) waveguide 60° bend implemented in a substrate-type InP/InGaAsP/InP planar photonic crystal based on a triangular array of air holes. The bend has been designed to provide high transmission over a large bandwidth. The investigated design improvement relies only on displacing holes while avoiding changing individual holes diameter in the interest of better process control (homogenous hole depth). Two-dimensional (2D) finite-element simulations were used to increase the relative transmission bandwidth from 18% to 40% of the photonic bandgap for unoptimized and optimized 60° bends, respectively. The 2D results were verified by means of rigorous three-dimensional (3D) finite-difference time-domain (FDTD) simulations. We show that excellent agreement between 2D and 3D simulations can be obtained, provided a small effective-index shift of −0.024 (−0.74%) and an imaginary loss parameter (ϵ'' = 0.014) is introduced in the 2D simulations. To demonstrate the applicability of our improved design, the bend was fabricated and measured using the endfire technique. A bending loss of 3 dB is obtained for the optimized *W*1 waveguide bend compared to more than 8 dB in the unoptimized case. © 2007 Optical Society of America

OCIS codes: 130.3120, 230.3120, 230.7370.

1. INTRODUCTION

Photonic crystals (PhCs) [1–3] are metamaterials based on a strong periodic modulation of the refractive index within the scale of the wavelength in one, two, or three dimensions. In recent years, two-dimensional (2D) planar PhC devices have been the object of extensive research, as they are relatively easy to fabricate with conventional semiconductor processing technology, in contrast to full three-dimensional (3D) PhCs. Planar PhCs [4] are based on vertical light confinement using index guiding in a slab waveguide and confinement in the horizontal plane provided by the PhC properties. The horizontal periodic structure is commonly manufactured by etching a triangular array of air holes, which provides a large photonic bandgap (PBG) for TE-polarized light. Removing one row of holes in a PhC lattice creates a W1 waveguide [5,6], which has the advantage of providing single-mode transverse waveguiding over a wide frequency range.

The waveguide bend is among the most basic integrated-optics building blocks. Low losses in conventional single-mode ridge-waveguide bends in the low refractive index contrast material system InP/InGaAsP are only obtainable by using sufficiently large bending radii (e.g., up to a few millimeters) in order to maintain total internal reflection. Smaller bending radii have been achieved with tightly confined photonic-wire waveguides [7], thanks to the much higher lateral index contrast, but single-mode operation requires very thin and lossy waveguides. Alternatively, as light guiding in PhC waveguides relies on the PhC properties [1] and not on total internal reflection, waveguide bending within one lattice constant (less than 1 μm) is feasible in these structures.

This work discusses the optimization of a 60° bend in a W1 waveguide in the substrate-type InP/InGaAsP material system with low refractive index contrast. For the triangular lattice, 60° bends are obtained from the lattice symmetry but are normally subject to light reflection owing to mode conversion and modal mismatch in the bending region. To enhance the transmission of the bends, various groups have explored the use of resonant cavities in the bending region formed [8] by varying hole sizes or replacing the hole at the outer edge of the bend by a more complex design [9,10]. Both approaches reduce process control (homogenous hole depth), as they require a more sophisticated lithography and etching process. A resonant cavity with uniform hole size is more favorable for fabrication, as, e.g., demonstrated for W3 (three missing rows of holes) bends [11]. Bends based on crystal dislocations whereby a global change of the crystal lattice is performed have also been explored [12], but such an approach is not easy to combine with the integration of other devices on the same lattice. In this work, we propose a single-mode W1 waveguide bend optimized for high bandwidth that relies only on the local displacement of individual holes. Although many investigations have been carried out on the optimization of PhC waveguides bends, to the best of our knowledge no systematic study of 60° bends relying on uniform hole size for simplified process control has been presented to date.

This paper is structured as follows. We first describe the optimization procedure of the 60° waveguide bend using 2D simulations. We then relate the optimized simulation results to full 3D computations. Finally, the results of the optical characterization of fabricated bend devices are presented to validate the optimization.

2. OPTIMIZATION PROCEDURE

The optimization of the bend is first performed in 2D, as the large size of the structure and the correspondingly large computation time makes 3D optimization impossible. 3D simulations are used only for verification and calibration of the 2D results. As long as dispersion effects are neglected, the scaling properties of the Maxwell equations allow the use of reduced frequency units $u=a/\lambda$ [1], where a is the lattice constant of the underlying triangular hole array. Our vertical three-layer slab waveguide consists of an InP cladding [300 nm], InGaAsP core [522 nm], and InP substrate. The 2D computations presented here are based on a frequency-dependent effective refractive-index [13] $n_{eff}(\lambda)$ computed semi-analytically to approximate the vertical slab waveguide [14]. Material dispersion is not considered here. We therefore lose the scalability of the PhC's, and it is necessary to specify the actual lattice constant $a=425$ nm of the device in the 2D simulations in order to calculate $n_{eff}(\lambda)$. The hole radius r is chosen to be $r=0.33a$, which provides a sufficiently large PBG width while keeping an acceptable interhole distance larger than ~80 nm [15] for the smallest lattice constant used for lithographic tuning [16]. Dispersion diagrams and transmission spectra are calculated using the plane-wave expansion method (using the software package MIT Photonic-Bands) [17] and the finite element (FE) software COMSOL [18], respectively.

Figure 1 presents the dispersion diagram of a W1 waveguide for $r=0.33a$. The PBG extends from $u=0.229-0.318$, while the W1 waveguide modes span the reduced frequency range $u=0.234-0.318$. Single-mode operation of the bend is possible only outside the frequency range covered by the odd mode ($u=0.258-0.270$) and below $u=0.309$, above which a higher-order waveguide mode appears. Only between $u=0.234-0.258$ (single-mode window B) and $u=0.270-0.309$ (single-mode window A) is the waveguide single-mode. In the multimode frequency region, mode conversion between the odd and even modes occurs at the bend owing to the symmetry breaking of the waveguide geometry [7]. Region A has a larger bandwidth than region B, which suffers additionally from difficult light incoupling from a trench access waveguide mode into the W1 waveguide owing to the large group-velocity mismatch in the slow-light regime [19].

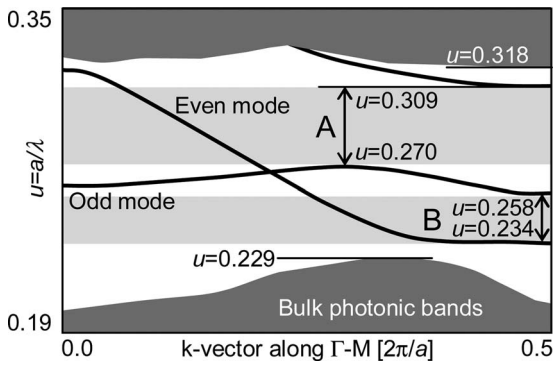

Fig. 1. Dispersion diagram of a W1 waveguide with $r=0.33a$ calculated in 2D with the plane wave expansion method [17] with a frequency-dependent $n_{eff}(\lambda)$. The PBG extends from $u=0.229-0.318$. For single-mode operation, the frequency range above the odd mode (A, $u=0.270-0.309$) has a larger bandwidth than the frequency range below (B, $u=0.234-0.258$).

The power transmission spectrum of the canonical 60° bend without optimization is presented in Fig. 2. For the FE method, the usual approach of power flux integration along a domain boundary to calculate the transmission cannot distinguish between the incoming and reflected waves, leading to inaccurate results in the case of reflections. Therefore we compute the transmission by power density integration over equally sized rectangles in the input ($P_{in}=P_{source}+P_{reflection}$) and output ($P_{out}=P_{transmission}$) waveguides (see Fig. 3). The power transmission T is then determined according to $T=2P_{out}/(P_{in}+P_{out})=P_{transmission}/P_{source}$, whereby we assume $P_{source}=P_{reflection}+P_{transmission}$. This method accounts correctly for reflections in lossless waveguides. Convergence with respect to the integration area ($8a$ long) has been ensured by comparing different detector sizes and positions. It should be noted that the method fails in the multimode region as the mode beating is larger than the integration area, leading to unphysical results that strongly depend on detector positions. However, since we are only interested in the single-mode regime (A or B), this does not affect the present investigation.

The unoptimized bend shows a narrow-band spectral response of the power transmission peaking at 99% near the dielectric band edge in the frequency range B around $u=0.245$ (Fig. 2). However, the 3 dB bandwidth is small and spans only the reduced frequency range of $u=0.239-0.255$. This corresponds to only 18% of the PBG width.

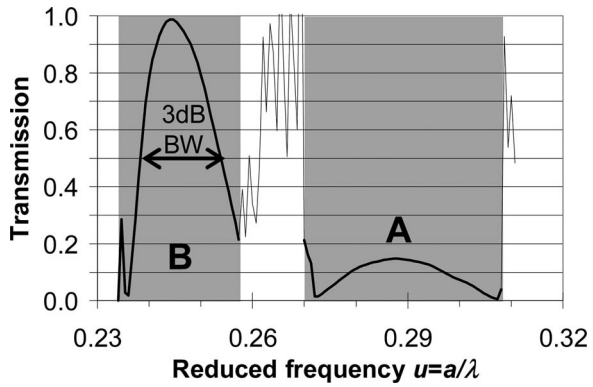

Fig. 2. Power transmission for the unoptimized bend computed by the 2D FE method. The gray regions in the transmission spectrum indicate the single-mode frequency range (B) below and (A) above the odd mode. High transmission in B can be achieved at the expense of a narrow 3 dB bandwidth that spans from $u=0.239-0.255$ (18% of the PBG, arrow). Outside the single-mode frequency ranges A and B, the simulation results are not meaningful owing to the long-range beatings between the modes, which makes the result dependant on the detector position.

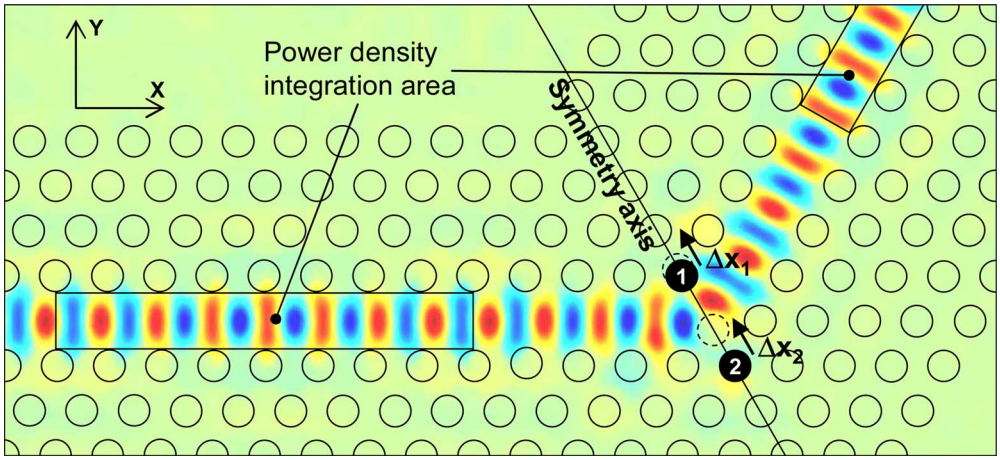

Fig. 3. (Color online) Labeling of the holes in the bending region. Only the location of the two black holes at the apex of the bend are parameterized within the optimizer. The arrows indicate the definition of the positive directions for the displacement values in Fig. 4. The dashed circles indicate the position of holes 1 and 2 after the optimization. The background shows the field plot (H_z) of the optimized bend at $u=0.294$. The power-density integration areas for the simulations are indicated by the rectangles.

Technological constraints have to be followed for an optimized design. To keep a good process latitude, we impose the following conditions on the optimization: (i) The shape and diameter of the holes shall remain unchanged; (ii) holes may not overlap and must maintain a minimum distance of 50 nm to avoid mask breakdown due to faceting [20]; (iii) the lattice constant must be kept fixed except in the bending region; and (iv) the bend must be symmetric in order to preserve reciprocity with respect to power transmission, meaning that the bending loss due to out-of-plane scattering should be independent of the propagation direction.

The coupling of the even and odd modes in the multimode region ($u=0.258-0.270$) cannot be prevented by design, as a 60° bend always breaks the transversal symmetry of the waveguide. Since the single-mode frequency range A is larger than B, it is more suitable for broadband power transmission. Therefore the optimization goal is to move the operating point into this frequency range.

As shown by means of a sensitivity analysis performed in [4], the holes that most strongly influence the transmission are the two holes at the apex of the bend (holes 1 and 2 in Fig. 3). We therefore restrict ourselves to a rigorous optimization of these two holes to limit computational cost. The requirement for symmetry and the restriction to only the two holes closest to the apex of the bend leaves two optimization degrees of freedom: moving the holes 1 and 2 along the symmetry axis of the bend (black line in Fig. 3). The same methodology as for the transmission spectra of the unoptimized bend (Fig. 2) was adopted. The step size for the optimization of Δx_1 and Δx_2 was chosen to be $0.04a$, corresponding to a hole position variation step of 17 nm for $a=425$ nm lattice constant. This value is a good trade-off between accuracy and calculation time. The maximal 3 dB and 1.5 dB bandwidths and the maximal power transmission in the upper single-mode window were used as optimization goals. As will be subsequently shown, all three goals can be fulfilled simultaneously.

Figure 4(a) shows the results of the 3 dB bandwidth optimization. A high transmission bandwidth ($\Delta u>0.036$, corresponding to 40% of the PBG) is achieved over a large range of hole displacements [white region in Fig. 4(a)] between $\Delta x_1=0a-0.18a$, and $\Delta x_2=0.66a-0.90a$ for holes 1 and 2, respectively. The fact that the area of maximized bandwidth lies along the diagonal in the $\Delta x_1-\Delta x_2$ plot suggests that the dominant dimension for the optimization is not the position of the individual holes alone, but the distance between the two holes. The position of hole 1 for which maximal transmission is achieved extends to up to $\Delta x_1=0.18a$, solely limited by the capability to manufacture closely spaced holes. On the other hand, for small negative displacement values Δx_1, the transmission at low frequencies inside the single-mode region A drops and the bandwidth shrinks. The useful optimization range for hole 2 is limited by transmission dips appearing in the frequency spectra region A, whereas the overall transmission remains high.

The 1.5 dB bandwidth and the maximal power transmission are also considered for the optimization. The 1.5 dB bandwidth shows similar behavior as shown for the 3 dB bandwidth in Fig. 4(a).

Figure 4(b) shows the results for the transmission optimization. The maximal lossless (i.e., $\varepsilon''=0$) transmitted power lies above 98% for the overall region where we simultaneously achieve high transmission bandwidth. Around $\Delta x_1=0.15a$ and $\Delta x_2=0.80a$ a broad 3 dB and 1.5 dB bandwidth (40% and 37% of the PBG, respectively) is achieved, while the distance between hole 1 and its nearest neighbor is still $0.19a$ (corresponds to 80 nm at $a=425$ nm) and offers sufficient process latitude. These displacement values were therefore chosen for the optimized bend.

To estimate the stability of the optimized design, the region around $\Delta x_1=0.15a$ and $\Delta x_2=0.80a$ was simulated with a finer resolution of $0.01a$. Over a range of $0.02a$ (corresponding to a position variation of 9 nm at 425 nm lattice constant, which is easily achieved using electron-beam lithography) in Δx_1 and Δx_2 around the chosen solution in each direction, the change in the 3 dB and

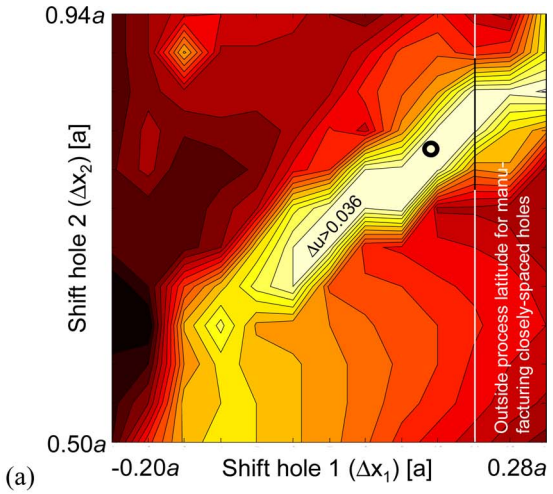

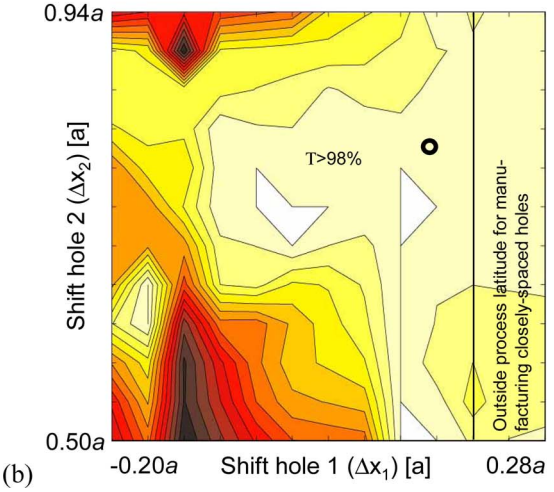

Fig. 4. (Color online) (a) 3 dB bandwidth as a function of the hole shifts Δx_1 and Δx_2. A large range of shifts (bright region) allows for maximal power transmission and large bandwidth ($\Delta u > 0.036$, corresponding to 40% of the PBG). Each darker level step represents a bandwidth reduction of $\Delta u = 0.02$. The plot for the 1.5 dB bandwidth looks very similar. (b) Maximal transmitted power within the upper single-mode window A as a function of the hole shift Δx_1 and Δx_2. Each darker level step represents a power level reduction of $T = 2\%$. The circles indicate the optimized position ($\Delta x_1 = 0.15a$ and $\Delta x_2 = 0.80a$).

1.5 dB bandwidths is smaller than ~5%. This validates the robustness and insensitivity of the optimized design.

Figure 5 presents the power transmission spectrum of the optimized bend. It shows a 3 dB transmission bandwidth of 40% ($u = 0.273 - 0.309$) of the PBG width, and with a maximum peak transmission of 99.4%. Also, as intended, the operation point is moved to the frequency range (A) above the odd mode. A high transmission is maintained over a large bandwidth, as demonstrated by a very broad 1.5 dB bandwidth of 37% of the PBG. For telecommunication wavelengths around 1500 nm, an implementation of the bend with a lattice constant $a = 425$ nm shows a 3 dB bandwidth spanning from 1375 to 1556 nm ($\Delta\lambda = 181$ nm). We attribute the improved performance of

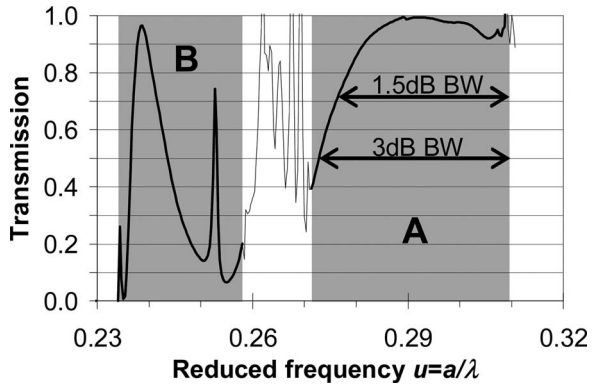

Fig. 5. Power transmission of the optimized bend computed with the 2D FE method. Hole 1 is displaced by $\Delta x_1 = 0.15a$ and hole 2 by $\Delta x_2 = 0.80a$ along the symmetry axis of the bend. The frequency range for high transmission is shifted above the odd mode, and the 3 dB bandwidth has increased from 18% to 40% of the PBG. Outside the single-mode frequency ranges A and B, the simulation results are not meaningful owing to the long-range beatings between the modes, which makes the result dependent on the detector position.

the optimized bend to the smoother bend apex and to the reduction of parasitic resonances in the frequency range of the transmission, caused by the cavity formed behind hole 2. Indeed, the bandwidth is often limited by the appearance of resonances in the above-mentioned cavity.

3. VERIFICATION BY 3D SIMULATIONS

The effective-index approach employed in the 2D simulations discussed above reduces the vertical confinement structure to a homogeneous effective-index of refraction for the 2D PhC's background material. This approach sacrifices detailed 3D information for a simpler, faster model. In this section we discuss the changes in the 2D model to analyze and compensate for the reduction in accuracy introduced by the effective-index simplification. For comparison, the 2D simulations are again performed with the FE method, whereas the 3D computations rely on an finite-difference time-domain algorithm. A filling factor of $r = 0.36a$ was used here, corresponding to the measured filling factor of the fabricated sample. With these real parameters, the PBG extends $u = 0.239 - 0.355$, and the upper single-mode frequency range A spans $u = 0.281 - 0.325$.

The 3D simulations show a maximal transmission of ~85% owing to out-of plane losses, which are not considered for the 2D optimization. Out-of-plane losses are now included in the 2D simulations by adding an imaginary permittivity to the air holes $\varepsilon_{hole} = 1 - i\varepsilon''$ [21,22]. Additionally, our analysis of the PhC bend shows a shift in the spectral responses of the 2D model toward longer wavelengths and smaller frequencies compared to the 3D full-wave simulations. This shift can be attributed to the different impact that the holes have on the mode structure in the 2D model and in the realistic planar 3D model, respectively. We believe that the true eigenfields of the 3D planar PhC structure are less confined to the underlying slab's core layer than the eigenmodes of the same but unperturbed slab, meaning that the effective refractive in-

dex (i.e., the background index) of the 2D model is slightly overestimated. The spectral deviation between the two PhC models decreases when dealing, e.g., with W1 waveguides and similar devices instead of a planar bulk PhC. Regarding our bend simulations, we have compensated for the aforementioned spectral deviation just by adding a correspondingly small correction to the effective refractive index $n_{eff,bend}(\lambda)=n_{eff}(\lambda)-\delta n$ of the background semiconductor material in our 2D model.

The free parameters ε'' and δn were varied to minimize the rms difference in transmission between the 2D and 3D simulations for the frequencies inside the single-mode window A. Figure 6 presents the 3D simulation of the power transmission spectrum and its corresponding 2D approximation. The optimal fit is found for $\varepsilon''=0.014$ and $\delta n=0.024$ (-0.74%). However, the optimum is quite broad. Only a 10% increase of the rms value results within the range of $\varepsilon''=0.06-0.26$ and $\delta n=0.018-0.028$. It should be mentioned that the fitted ε'' does only account for intrinsic losses. Real losses due to nonperfect hole cylindricity will increase its value. The introduction of the n_{eff} shift and loss into the 2D computations does not introduce new features (dips, cutoff), but shifts the spectral features along the frequency axis and reduces the transmission to the 3D level, respectively. Therefore we conclude that 2D simulations are indeed sufficient to optimize the design of the bend, although for optimal matching to 3D simulations, phenomenological correction parameters to n_{eff} have to be introduced.

4. BEND FABRICATION AND CHARACTERIZATION

Optimized and unoptimized bend designs, as well as reference W1 waveguides, were fabricated using our in-house technology to verify the predicted transmission enhancement gained by the optimization. A vertical layer structure consisting of an InP top cladding (300 nm, $n=3.17$), an InGaAsP core (522 nm, $n=3.35$) and an InP bottom substrate cladding ($n=3.17$) was used. The wafer was grown by metal-organic vapor phase epitaxy. The pattern was written by EBL into a poly(methyl methacrylate) resist [15] and transferred to a SiN_x hardmask by dry etching [23]. The hardmask is used to etch the InP/InGaAsP/InP layer stack by inductively coupled plasma reactive ion etching with a $Cl_2/Ar/N_2$ chemistry [20]. Holes are up to 3.5 μm deep. The filling factor of the fabricated device was validated using scanning electron microscope inspection and found to be higher (46.8%, $r=0.36a$) than designed, owing to fluctuations of the fabrication process.

Measurements were performed using the endfire technique [4], whereby light is generated off-chip by tunable laser sources and coupled into the chip facets by a polarization-maintaining lensed fiber. The bandwidth of the sources extends from $\lambda=1470$ nm to $\lambda=1630$ nm. Therefore, to measure the full bandwidth of the bend, lithographic tuning [16] was applied, whereby scaled devices with lattice constants ranging from $a=375$ nm to $a=500$ nm in 25 nm steps were fabricated, covering the entire PBG. Between the cleaved facets and the PhC structure comprising bend, the light is guided by conventional ridge access waveguides (Details about the access waveguide structure can be found in [24]). To avoid a nonperpendicular outcoupling of the light at the opposite cleaved facet, a curved waveguide section with a large bending radius after the PhC bend is introduced. This smooth bend undoes the PhC bend's light deflection and guides it back to the perpendicular orientation. The access waveguide structures are the same for the optimized and nonoptimized bend, to allow for comparison. After propagation through the device, the signal is collected at the output by a microscope objective and measured by an InGaAs power meter. A pinhole before the detector shields it from stray light.

Figure 7 presents the transmitted power for the fabricated structures. The upper single-mode transmission band for the fabricated filling factor $r=0.36a$ spans from $u=0.281$ to $u=0.325$ (gray region). Taking a W1 waveguide as a reference, the optimized bend shows a decrease

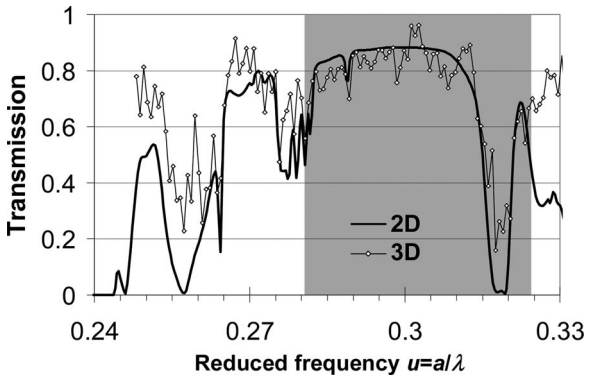

Fig. 6. Simulated power transmission spectra for the bend implemented with $r=0.36a$. The gray region indicates the single-mode frequency range A ($u=0.281-0.325$). A loss term $\varepsilon''=0.014$ and effective-index shift $\delta n=0.024$ (-0.74%) are introduced in the 2D simulation to optimally match the 3D simulations. As the area-integration method for the transmission calculation fails for a simulation including losses, power flux detectors are used at the input and output, and the transmission is calculated according to $T=P_{out}/P_{in}$. As the reflections are low, the result is believed to be accurate within the single-mode transmission window.

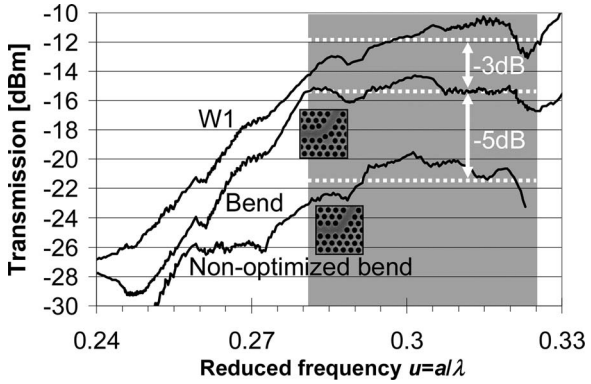

Fig. 7. Measured transmitted power through optimized and unoptimized bends in comparison with a reference $W1$ waveguide of the same length. The gray region indicates the single-mode frequency range above the odd mode ($u=0.281-0.325$). An increase of about 5 dB has been achieved by the optimization. The optimized bend retains a device loss of 3 dB.

of 3 dB in transmission within the relevant single-mode window. In comparison with the unoptimized bend, however, it improves the transmission by about 5 dB.

To understand the measurement results, we simulated the fabricated structure by FE, including losses in the 2D simulation (applying the ε'' model [21,22]) based on the fabricated design. We again use the power density integration method to calculate the transmission. However, this method becomes inaccurate, as $P_{source} \approx P_{reflection} + P_{transmission}$ is only fulfilled approximately. This inaccuracy allows only qualitative comparisons with the measurements. The ε'' value was chosen higher (ε'' up to 0.4) than the value found in Section 3, as additional losses arising from nonperfectly fabricated holes have to be included. For all simulated devices, the distinct frequency features become smoothed with higher ε'' value. This smoothing of the power transmission spectrum is also present in the measurement, as no distinct frequency features are visible.

Comparing the simulated optimized and unoptimized bends, we estimate the performance improvement to be up to 7.5 dB in the frequency window A, independent of the chosen ε'' value. This agrees qualitatively with the measurement results.

In the measurement, the optimized bend shows a lower transmission compared to the W1 waveguide of the same length. This contradicts the (lossless) results of the optimization. Including losses in the simulation, we found that the W1 waveguide has a higher power transmission than the optimized bend, but only by around 1 dB (for $\varepsilon'' \approx 0.4$). As the attenuation increases with increasing ε'' value, we believe that the bend shows increasingly lower transmission than the W1, because the mode penetrates deeper into the holes at the apex of the bend than into the holes along the W1 waveguide. This assumption is supported by the measured lower transmission through the bend and the simulations including losses.

5. CONCLUSION

We showed the full optimization cycle of a 60° waveguide bend in InP/InGaAsP/InP, restricting the optimization to local hole displacements for improved process control. By shifting the holes along the symmetry axis of the bend, an optimized design was found, resulting in an improvement of the 3 dB bandwidth from 18% to 40% of the PBG width, with a maximum power transmission for the lossless 2D model of 99.4%. Owing to out-of-plane losses, the maximal transmission drops to ~85% for the 3D simulations. We showed that by introducing an imaginary part to the refractive index of the holes ($\varepsilon''=0.014$) and an n_{eff} shift to the semiconductor ($\delta n=0.024$) we can adapt the computationally less intensive 2D simulations to the 3D results. As these measures only shift and lower the transmission spectrum but do not introduce new frequency features, we conclude that 2D simulations are sufficient for the optimization of a device. The measurement of the fabricated optimized bend showed an increase in the transmission of 5 dB compared to the unoptimized bend, leading to a bending loss of 3 dB.

REFERENCES

1. J. D. Joannopoulos, R. D. Meade, and J. N. Winn, *Photonic Crystals—Molding the Flow of Light* (Princeton U. Press, 1995).
2. E. Yablonovitch, "Inhibited spontaneous emission in solid-state physics and electronics," Phys. Rev. Lett. **58**, 2059–2062 (1987).
3. S. John, "Strong localization of photons in certain disordered dielectric superlattices," Phys. Rev. Lett. **58**, 2486–2489 (1987).
4. K. Rauscher, "Simulation, design, and characterization of photonic crystal devices in a low vertical index contrast regime," dissertation ETH 16516, electrical engineering (ETH Zurich, 2006).
5. T. Baba, "Light transmission in photonic bandgap waveguides and photonic band crystals," Proc. SPIE **4870**, 265–271 (2002).
6. E. Chow, S. Y. Lin, J. R. Wendt, S. G. Johnson, and J. D. Joannopoulos, "Quantitative analysis of bending efficiency in photonic-crystal waveguide bends at lambda=1.55 μm wavelengths," Opt. Lett. **26**, 286–288 (2001).
7. C. Xudong, C. Hafner, R. Vahldieck, and F. Robin, "Sharp trench waveguide bends in dual mode operation with ultra-small photonic crystals for suppressing radiation," Opt. Express **14**, 4351–4356 (2006).
8. A. Chutinan, M. Okano, and S. Noda, "Wider bandwidth with high transmission through waveguide bends in two-dimensional photonic crystal slabs," Appl. Phys. Lett. **80**, 1698–1700 (2002).
9. L. H. Frandsen, A. Harpøth, P. I. Borel, M. Kristensen, J. S. Jensen, and O. Sigmund, "Broadband photonic crystal waveguide 60° bend obtained utilizing topology optimization," Opt. Express **12**, 5916–5921 (2004).
10. B. Miao, C. Chen, S. Shi, J. Murakowski, and D. W. Prather, "High-efficiency broadband transmission through a double-60 bend in a planar photonic crystal single-line defect waveguide," IEEE Photonics Technol. Lett. **16**, 2469–2471 (2004).
11. S. Olivier, H. Benisty, M. Rattier, C. Weisbuch, M. Qiu, A. Karlsson, C. J. M. Smith, R. Houdré, and U. Oesterle, "Resonant and nonresonant transmission through waveguide bends in a planar photonic crystal," Appl. Phys. Lett. **79**, 2514–2516 (2001).
12. S. Xiao and M. Qiu, "Study of transmission properties for waveguide bends by use of a circular photonic crystal," Phys. Lett. A **340**, 474–479 (2005).
13. M. Qiu, "Effective index method for heterostructure-slab-waveguide-based two-dimensional photonic crystals," Appl. Phys. Lett. **81**, 1163–1165 (2002).
14. http://wwwhome.math.utwente.nl/~hammer/oms.html.
15. R. Wüest, F. Robin, C. Hunziker, P. Strasser, D. Erni, and H. Jäckel, "Limitations of proximity-effect corrections for electron-beam patterning of planar photonic crystals," Opt. Eng. **44**, 043401 (2005).
16. R. Ferrini, D. Leuenberger, M. Mulot, M. Qiu, J. Moosburger, M. Kamp, A. Forchel, S. Anand, and R. Houdré, "Optical study of two-dimensional InP-based photonic crystals by internal light source technique," IEEE J. Quantum Electron. **38**, 786–799 (2002).
17. S. G. Johnson and J. D. Joannopoulos, "Block-iterative frequency-domain methods for Maxwell's equations in a planewave basis," Opt. Express **8**, 173–190 (2001).
18. http://www.comsol.com.
19. Y. A. Vlasov and S. J. McNab, "Coupling into the slow light mode in slab-type photonic crystal waveguides," Opt. Lett. **31**, 50–52 (2006).
20. P. Strasser, R. Wüest, F. Robin, D. Erni, and H. Jäckel, "A detailed analysis of the influence of an ICP-RIE process on the hole depth and shape of photonic crystals in InP/InGaAsP," J. Vac. Sci. Technol. B **25**, 387–393 (2007).
21. H. Benisty, D. Labilloy, C. Weisbuch, C. J. M. Smith, T. F. Krauss, D. Cassagne, A. Béraud, and C. Jouanin, "Radiation losses of waveguide-based two-dimensional photonic crystals: positive role of the substrate," Appl. Phys. Lett. **76**, 532–534 (2000).
22. R. Ferrini, R. Houdré, H. Benisty, M. Qiu, and J. Moosburger, "Radiation losses in planar photonic crystals:

two-dimensional representation of hole depth and shape by an imaginary dielectric constant," J. Opt. Soc. Am. B **20**, 469–478 (2003).
23. R. Wüest, P. Strasser, F. Robin, D. Erni, and H. Jäckel, "Fabrication of a hard mask for InP based photonic crystals: increasing the plasma-etch selectivity of poly(methyl methacrylate) versus SiO_2 and SiN_x," J. Vac. Sci. Technol. B **23**, 3197–3201 (2005).
24. R. Wüest, "Nanometer-scale technology and near-field characterization of InP-based planar photonic-crystal devices," Dissertation 17146, Electrical engineering (ETH Zurich, 2007).